

Simulating 3-D Single Gas Bubble Growth in a Polymer Melt Using Multi-Phase SPH

Burak Kaan Cirpici¹, Benedict D. Rogers² & Yong C. Wang²

¹Department of Civil Engineering, Corlu Engineering Faculty, Namik Kemal University, Tekirdag
59860, Turkey

²Modelling and Simulation Centre (MaSC), School of Mechanical, Aerospace and Civil Engineering,
University of Manchester, Manchester M13 9PL, UK

Corresponding author: bkcirpici@nku.edu.tr

Abstract: Modelling of the expansion of 3-D single bubble using a multi-phase model has been developed for GIVE APPLICATION AREA with the potential of a meshless numerical simulation method, Smoothed Particle Hydrodynamics (SPH), and the consideration of the surface tension between phases and viscosity effect of the polymer melt surrounding the bubble. Mainly, bubble growth in the polymer material occurs because of the mass conversion (mass loss) from the polymer melt to gas due to heat such as fire. This mass conversion drives the expansion process of the gas bubble by increasing the pressure inside. To represent the mass transfer from the polymer melt to the bubble, this paper proposes a novel algorithm to increase number of SPH gas particles inside the bubble during the simulation. The present paper aims to explain this new developed method including particle shifting scheme identifying the main challenges of dynamic and non-spherical bubble modelling which have a nonlinear multi-phase behaviour. In order to develop stable simulations for the multi-phase bubble growth in isothermal conditions in millimeter scale, surface tension effects have been scaled according to the Capillary number. The insertion of the new gas particles into the bubble centre has been performed at regular intervals to identify the influence of time period of particle insertion. The predicted results from the numerical study have been compared with the well-known analytical solution for single bubble growth for final bubble radius and bubble growth rate. Time step analysis has also been performed to show the numerical stability for this kind of bubble growth simulation. The importance of the particle shifting scheme has also been addressed for simulating bubble growth in this multi-phase problem.

Keywords: Bubble growth, Smoothed Particle Hydrodynamics (SPH), Multi-phase, Surface tension, Viscosity.

1 Introduction

The foaming of a polymer melt is an important issue for applications such as insulation, personal care and fire retardation. The main feature, which has an effect on the quality of the thermoplastic foam product, is the cell size distribution (CSD). Many factors influence the final CSD of a foam, including bubble nucleation, growth, deformation, possible coalescence and bursting, while each of these depends on many sub-factors such as temperature, pressure, blowing agent and the use of nucleating agents [1].

The foaming process, dominated by the dynamics of the gas-liquid interface and using physical blowing agents, is a complex process which consists of three main stages. The first is “nucleation”, where the gas in the gas-liquid mixture diffuses into gas clumps and begins to form bubbles. The second is essentially “bubble growth”, where bubbles grow due to a gas source from the liquid or smaller neighboring bubbles. The third step is “coarsening”, where the bubbles come together and combine into larger bubbles [2]. Although numerous works have been conducted on the theoretical study of bubble growth including experiments, only a limited number of studies have reported the issue of the dynamic behavior of bubble growth in the molten polymer. It is mentioned in the work of Tuladhar and Mackley [3] that the classical and well-known theory of nucleation is based on Gibbs free energy, which is appropriate for creating a void in a liquid and assumes that the critical bubble is in equilibrium in terms of mechanical and thermodynamic properties. In their model, bubbles larger than the critical bubble size keep growing while smaller ones dissolve. As the bubble growth is mainly related to the pressure, the growth does not continue infinitely because the concentration of the dissolved gas $c_r(t)$ in the surrounding polymer melt also reduces with respect to time. Hence, the rate of bubble growth is a function of the polymer viscosity, diffusivity of the gas (mass conversion from liquid to gas) and pressure inside the bubble. In reality and for any numerical model for multi-bubble growth, expanded bubbles that are in close proximity to another bubble or bubbles cannot grow infinitely, since only a finite supply of gas is available for the growth [4]. The prediction of the nucleation process is therefore difficult, but if it occurs, bubble growth is controlled by the fundamental laws where the pressure of the gas within the bubble provides a driving force to expand the bubble whereas the viscosity of the polymer and surface tension of the bubble wall provide opposing forces (resistance) to bubble growth. This physical phenomenon of bubble growth in Newtonian fluids is based on the simultaneous mass and momentum transfer. The schematic of a single bubble can be shown in Figure 1.

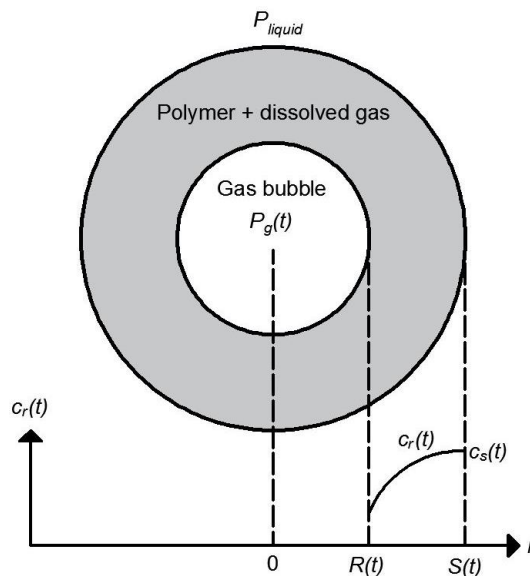


Figure 1: Schematic diagram of a single bubble growth model [3]

With many variables influencing the bubble modelling simultaneously, sensitivity studies for the parametric values should be conducted [3]. For instance, some of those parameters are initial bubble radius, influence cell radius, melt viscosity, diffusion coefficient, initial gas concentration, etc. Initial bubble size is directly related to the surface tension, so as the bubble size increases, the importance of the surface tension decreases. The important parameters for the bubble growth in the polymer melt are the viscosity, surface tension and the pressure increase inside the bubble, and they can be modelled using other computational approaches. With the aim of understanding the mechanisms, grid-based numerical methods for computational fluid dynamics have been used for modelling this kind of multi-phase problem including simulating the motion of a single bubble rise in a liquid using Front Tracking Method [5], modelling a single droplet's drop on to a liquid interface using the Level Set Method [6],

numerical predictions for 2-D bubble collapse within a viscous fluid surrounded by a rigid boundary using Marker Particle Method [7], simulating single condensing bubble behavior in a cooled flow using Volume-of-Fluid Method [8] and development of 3-D multiple bubble rising under buoyancy force considering bubble-bubble interaction in a viscous incompressible fluid using the Lattice Boltzmann Method [9]. These approaches can be broadly classified as Eulerian, involving variation of flow quantities at fixed points in space, and Lagrangian where the flow properties can move in space and time. [10]. For changing grid methods such as the finite element method (FEM), mesh generation is also necessary to simulate the flow, because mass, momentum and energy are transported with the movement of mesh cells. However, it can be time consuming when the objects have large deformations and distortions. It may even introduce inaccurate results [11]. Points in the mesh or grid need to be destroyed in a case where significant deformation appears or sharp changes of geometry occur, such as in a violent fluid flow. Therefore, these grids need to be remeshed or refined for these kinds of problem, which leads to a computationally expensive process.

The Smoothed Particle Hydrodynamics (SPH) method is foreseen as being able to capture these nonlinear phenomena. As a meshless method, SPH method obtains approximate numerical solutions to the set of equations representing the dynamics by replacing the medium with a set of particles. The particles are free to move according to the governing dynamics and interact with each other by means of overlapping influence areas known as smoothing kernels or weighting functions. These kernels have a characteristic spatial distance, generally known as the “smoothing length”, which is represented by “ h ”. The physical property of any particle can be estimated by summing weighted contributions of all the surrounding particles that are located within the radius of influence (support) of the kernel. The advantages of this method compared with other computational methods are due to:

- (i) No mesh or potentially expensive grid is required to compute spatial derivatives because of its meshless nature.
- (ii) The conservation of mass without extra computational process is exact since the mass of each particle remains constant.
- (iii) An important advantage directly relevant to this study is that it is possible to deal with interface problems, since each material is described by its own set of particles.

This meshless method was initially developed for solving astrophysical problems [12, 13]. It is still in use for simulations of star formation [14] and coalescence of black holes [15]. In the past two decades, the method has been used extensively to tackle fluid dynamics problems, especially free-surface flows [16], [17], [18] as well as solid dynamics problems [19], and brittle solids [20]. The range of applications of SPH is very broad and varied, encompassing areas such as solid and fluid mechanics, heat conduction [21], fracture mechanics [19], fluid-solid modelling [22], modelling of water waves, sloshing, etc. [23]. Multi-phase models such as those encountered here, and will be discussed in Section 2.2, have also been developed with the aid of the meshless nature of the SPH method [24].

There is currently no established model for the simulation of bubble growth in a liquid by SPH and this work aims to fill this knowledge gap. In this work, the main interest lies in the modelling of a gas bubble in the surrounding fluid. Therefore, the model is considered as multi-phase modelling. A model of this kind of multi-phase flow is quite complex and includes an interface between the air and fluid phase with numerous discontinuities and stability problems. Moreover, different models (i.e. surface tension, no-penetration force), correction methods (e.g. shifting method) and the new particle generation method have been added to develop a robust modelling scheme and to improve the accuracy of the modelling.

This paper describes the physics behind gas bubble growth process with its significant challenges that should be overcome to make SPH a feasible method. The results obtained from the SPH simulations are compared with the analytical solution for single bubble growth developed by Patel [25] in terms of final bubble radius and bubble growth rate. Moreover, a novel algorithm to represent the mass transfer for the bubble growth including the particle shifting methodology is represented herein.

2 Bubble Expansion Modelling Methods

The problem of bubble nucleation and growth inside foams plays an important role in the chemical industry. The well-known single bubble growth model is of Patel [25]. The numerical results from SPH will be compared with those results obtained from analytical method.

2.1 Governing Bubble Growth Equation

Patel [25] developed an analytical bubble growth model in a viscous fluid by considering the diffusion from the polymer liquid to the gas phase. The assumptions in that model were:

- The system is isothermal and a thermodynamic equilibrium exists continuously between the gas pressure inside the bubble and polymer-gas solution at the interface.
- All physical properties of the liquid and gas are constant. This assumption is also applicable for SPH bubble growth modelling except that the density changes according to the conservation of mass.
- The normal stresses at the interface are the surface tension and viscosity, neglecting the inertial terms.
- The rate of the bubble's growth is related to the pressure increase inside the bubble, whereas ambient pressure P_a is assumed to be constant,

$$\frac{dR}{dt} = R \left(\frac{P_g - P_a - 2\sigma_s/R}{\eta_o} \right) - 3P_g \left(\frac{\dot{R}}{R} \right) \quad (1)$$

where P_g and P_a are the gas pressure inside the bubble and the ambient pressure respectively. R is the radius of the bubble, \dot{R} is the bubble growth rate, σ_s is the surface tension coefficient and η_o is the viscosity of the polymer liquid. It is assumed that the initial bubble radius should be greater than the critical bubble radius, R_{cr} , which comes from the Young-Laplace equation,

$$R_{cr} = \frac{2\sigma_s}{P_{g_o} - P_a} \quad (2)$$

As this bubble growth model describes a single bubble growth due to the assumption of unlimited supply of blowing agent, it does not consider the influence of surrounding bubbles. Therefore, this model over predicts the actual bubble growth in polymer foaming. Another shortcoming of this model is that the polymer liquid is assumed to be a Newtonian fluid while the bubble forming in polymer foams behaves as a non-Newtonian fluid and the physical properties such as viscosity and surface tension change with time. However, this model is still applicable to this kind of modelling of bubbles by making necessary changes to the assumptions.

Figure 2 shows a sketch of the main quantities involved in bubble growth where the radius of the bubble is R . The main driving force for bubble growth is the increased gas pressure inside the bubbles (P_g). The resistance forces, which control the bubble growth process, are due to the viscosity (η) and surface tension force (F_s) due to surface tension at the interface. These forces act on the interface, which has infinitesimally small thickness, shown in Figure 2 by zooming in to the interface.

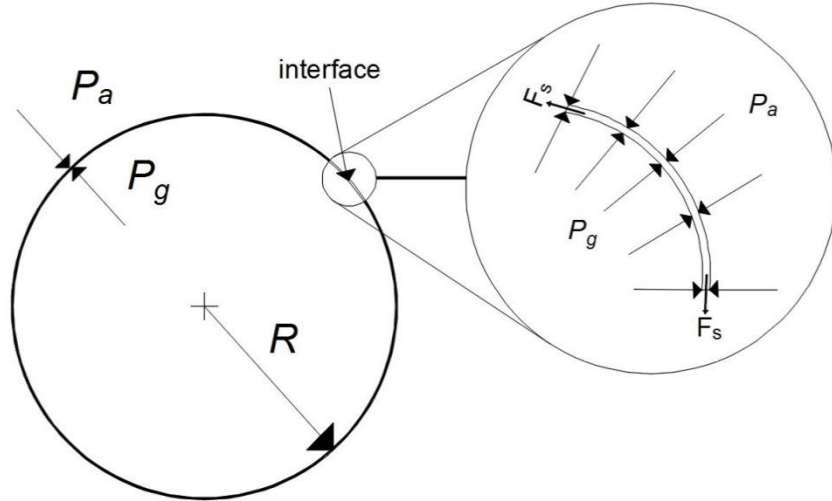


Figure 2: A sketch of the forces acting on a bubble

2.2 Multi-Phase SPH Modelling

As mentioned in the previous section, SPH is a Lagrangian method which enables the simulation of multi-phase flows such as explosive multi-phase pipe flow, wave breaking, and air bubble formation (gas expansion) in a liquid. It can be a difficult and complex task to apply the Eulerian grid-based methods to these kinds of multi-phase flow simulation, as the creation of mesh requires a significant amount of time, complex algorithms and high quality computational resources [26].

Extensive research methods with the SPH scheme have already been proposed for multi-phase modelling, including both liquid-gas and liquid-liquid flows. One of the most attractive features of SPH is to include more than one fluid with a separate set of particles in each phase by assigning different equations of state [27]. However, the accuracy of the multi-phase modelling results is greatly dependent on the ratio of their hydrodynamic properties such as density and viscosity [28], [29].

One of the first multi-phase SPH schemes examined the motion of dust and gas by movement of the dust into a static gas phase [30]. Shortly after, Monaghan and Kos [16] proposed a multi-phase SPH for the interaction of multiple fluids to simulate the gravity current free-surface problems with a ramp. The results were satisfactory, with a correction to the velocity keeping the particles more orderly and preventing the particle penetration. As the density ratio between the fluids was small, using the classical SPH formulation without applying any corrections at the interface could be acceptable. However, when simulating large density ratios (e.g. 1:1000), several instability problems in the region between the two substances can occur due to the high density gradient at the interface and the presence of density in the denominator of SPH summations. Colagrossi and Landrini [24] proposed one of the first treatments for this problem by modifying the expressions for SPH gradients.

A different approach was conducted by Hu and Adams [28], in which the density is only affected by the particle's own volume rather than the volumes of neighboring particles. They also expressed the shear stress contribution in terms of the color function (see Section 3.2) such that the surface tension term could be evaluated using that color function.

The previous work was followed by the incompressible model developed by the same authors [31]. A constant density approach has been introduced by correcting the density errors at a half-time step to simulate the flows with high density ratios (i.e. a density ratio of 100 or more). As this more recent incompressible model requires greater computational resources, the method of Hu and Adams [28] has been applied directly to surface tension modelling, and the bubble growth test case.

Grenier et al. [32] proposed a multi-fluid model combining the viscosity and surface tension of Hu and Adams [28] based on the specific volume of particle approach with Colagrossi and Landrini [24] scheme. The method of Grenier et al. [32] was used to simulate an air bubble rising in water (multi-phase flow) and also gravity currents (free-surface flows).

Similar to that used by Grenier et al. [32], a repulsion term is proposed for the lighter phase where the speed of sound is larger than that of the denser fluid (i.e. the ratio of speed of sounds is around 3) to simulate the multi-phase simulations [33]. This was later improved by involving the free-surface problem with no rigid boundaries being applied to non-linear oscillation of the fluids, the simulation of waves at the interface between two fluids, the Rayleigh-Taylor instability test case and simulating the gravity currents with density ratios of 2-30 [34].

In recent years, SPH has been applied to simulate the phenomena of bubbles rising and multiple bubbles coalescing in viscous fluids in 3-D [35]. Although SPH is becoming an increasingly popular method for free-surface flows (i.e. single phase flows), it can suffer from non-physical particles mixing at the interface of immiscible phases due to the current SPH formulations for multi-phase flows. Szwec et al. [36] has also studied the single bubbles rising through viscous fluids by choosing the speed of sound carefully to set the incompressibility of the fluid in order to minimize the density fluctuations due to the high density ratio between fluids. Similar care has also been taken in the simulation of bubble growth in this study.

3 SPH Model – SPHysics

3.1 Governing Equations

SPH modelling of gas bubble growth in a polymer liquid has been implemented using the SPHysics FORTRAN open-source code as a platform [37]. The SPH method is expressed by a local interpolation for set of particles where the physical properties of the particles such as mass m_i , density ρ_i , pressure P_i , velocity v_i and volume V_i are estimated and updated for every time step.

The formulation of the SPH method is composed of two main steps. The first is the *integral representation* (kernel approximation) of field functions and the second is the *particle approximation*.

The discrete or particle representation of an arbitrary function is approximated by summing up the function values of the nearest neighbor particles in the interpolation region.

The integral interpolation of a function A at position r is described as [38]:

$$A(\mathbf{r}) = \int A(\mathbf{r}')W(\mathbf{r} - \mathbf{r}', h)d\mathbf{r}' \quad (3)$$

where $W(\mathbf{r} - \mathbf{r}', h)$ is the smoothing kernel function, $\mathbf{r} - \mathbf{r}'$ is the interpolation distance and h is the smoothing length. The smoothing length defines the extent of the kernel with the radius of each kernel often set to be twice the smoothing length as shown in Figure 3. The particles outside the radius of influence have no effect on the influence domain. The region inside the radius of influence is called the compact support of the kernel. In SPHysics, a smoothing length of $h = 1.3\Delta x$ is used where Δx is the initial particle distance. This value provides a good correlation between sufficient number of particles in the support domain and accuracy.

A kernel function can be expressed in a general equation as [39]:

$$W(r_{ij}, h) = \frac{1}{h^d} f\left(\frac{r_{ij}}{h}\right) \quad (4)$$

where d is the number of dimensions, r_{ij} is the interpolation distance between 2 particles i and j , and f is the function.

For the kernel function, the cubic spline kernel has been chosen in the current developed bubble growth model as it has been found computationally efficient with the compact support [40]:

$$W(r_{ij}, h) = \alpha_d \begin{cases} 1 - \frac{3}{2}q^2 + \frac{3}{4}q^3 & 0 \leq q \leq 1 \\ \frac{1}{4}(2 - q)^3 & 1 \leq q \leq 2 \\ 0 & q \geq 2 \end{cases} \quad (5)$$

where $q = \frac{r_{ij}}{h} = \frac{r_i - r_j}{h} \geq 0$ and r_{ij} is the distance between the particles. α_d is the normalisation factor for the kernel to ensure the integral of the kernel itself reproduces the unity which is defined as $1/h$, $10/(7\pi h^2)$ and $1/(\pi h^3)$ for the cubic spline kernel in one-, two- and three-dimensional space respectively.

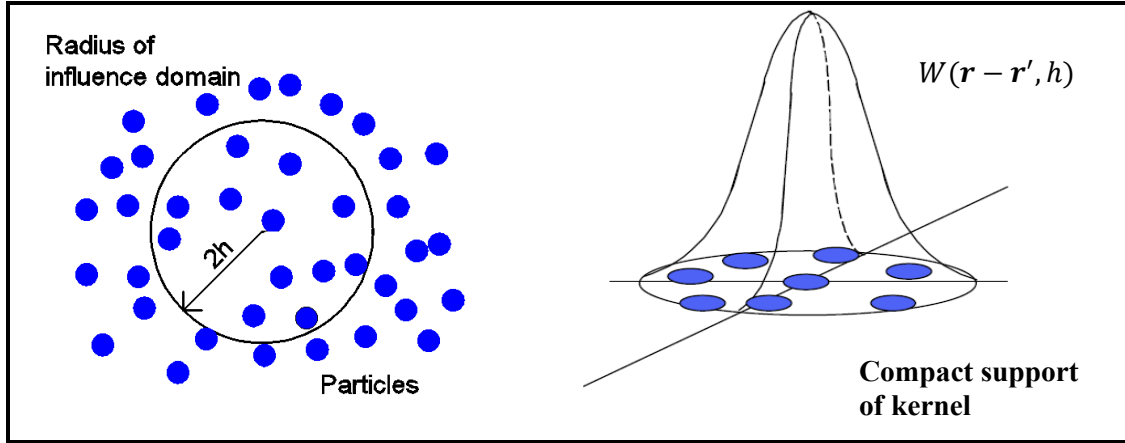


Figure 3: Kernel and its support domain

The integral interpolant is approximated by a summation at particle i as:

$$A(\mathbf{r}) = \sum_i m_j \frac{A_j}{\rho_j} W_{ij} \quad (6)$$

where ρ_j is the density of particle j ($j = 1, 2, 3, \dots, N$) and N is the number of particles within the support domain, m_j is the mass of particle j . $W_{ij} = W(|\mathbf{r}_i - \mathbf{r}_j|, h)$ is the kernel function with $r_{ij} = |\mathbf{r}_i - \mathbf{r}_j|$ is the distance between particles i and j .

Due to consideration of the infinitesimally small fluid element, the equation is obtained in partial differential equation form. The final version of the continuum equations are often written with the divergence term on the right hand side as:

$$\frac{D\rho}{Dt} = -\rho \nabla \cdot \mathbf{v} \quad (7)$$

$$\frac{D\mathbf{v}}{Dt} = -\frac{1}{\rho} [\nabla p - \nabla \cdot \boldsymbol{\tau}] + \mathbf{g} \quad (8)$$

where $\boldsymbol{\tau}$ is the shear stress tensor and \mathbf{g} is gravitational force vector.

The conservation of mass being solved is:

$$\frac{D\rho_i}{Dt} = \sum_{j=1}^N m_j \mathbf{v}_{ij} \cdot \nabla_i W_{ij} \quad (9)$$

where $\mathbf{v}_{ij} = \mathbf{v}_i - \mathbf{v}_j$, which is the relative velocity of particles i and j .

In this bubble growth model, laminar viscosity, Π_{ij} proposed by Morris et al. [39] is appropriate to represent the processes in a physically more appropriate manner as this flow case is low Reynolds number flow.

The conservation of momentum is formed by including the laminar viscosity Π_{ij} and surface tension term \mathbf{f}_s as:

$$\frac{D\mathbf{v}_i}{Dt} = - \sum_{j=1}^N m_j \left(\frac{P_i + P_j}{\rho_i \rho_j} + \Pi_{ij} \right) \nabla_i W_{ij} + \mathbf{f}_s \quad (10)$$

where gravitational force (g) is assumed to be zero in the developed model and \mathbf{f}_s is the surface tension term explained in the next section. Π_{ij} the viscosity term is given by,

$$\Pi_{ij} = - \frac{2v_{ij}}{\bar{\rho}_{ij}} \frac{\mathbf{r}_{ij}}{(|\mathbf{r}_{ij}|^2 + \eta^2)} \quad (11)$$

with

$$\bar{\rho}_{ij} = \frac{\rho_i + \rho_j}{2} \quad (12)$$

$$v_{ij} = \frac{v_i \times v_j}{v_i + v_j} \quad (13)$$

η is the constant and is equal to $0.01h$.

To link the density and pressure, a compressible equation of state formulation for quasi-incompressible SPH flows first introduced by Morris et al. [39] has been used since it is computationally faster without resulting in large pressure fluctuations. Small density variation can cause that large pressure fluctuations and unstable simulations as the developed model is not a static bubble case.

$$P = c_s^2(\rho - \rho_o) \quad (14)$$

Conservation of mass and momentum equations has been integrated in time using a second-order predictor-corrector time integration scheme with a variable time step algorithm [41].

3.2 Surface Tension

Surface tension can be explained as the resistance force of the fluid against extension of a surface. Surface tension forces are as a result of unbalanced molecular dynamic forces at the free surface between two different immiscible fluids such as polymer-air in this study. In order to model the surface tension force, the continuum surface force (CSF) is applied in the momentum equation of the particles based on the flow geometry [42]. In the CSF model, surface tension is transformed into a force per unit volume, \mathbf{F}_s with the following equation:

$$\mathbf{F}_s = \mathbf{f}_s \delta_s \quad (15)$$

where $\delta_s = |n|$, a normalised function (the surface delta function) and \mathbf{f}_s is the force per unit area given by:

$$\mathbf{f}_s = \sigma_s \kappa \hat{\mathbf{n}} + \nabla_s \sigma_s \quad (16)$$

where σ_s is the surface tension coefficient, $\hat{\mathbf{n}}$ is the unit normal to the interface, κ is the curvature of the interface ($\kappa = -\nabla \cdot \hat{\mathbf{n}}$), ∇_s is the surface gradient (it will be neglected as surface tension is assumed to be constant throughout the fluid).

Figure 4 shows the sketch of continuum surface force acting at the interface of an air bubble. Contour colorings separate the different fluids with color function values of C_i^1 and C_i^2 as,

$$C_i^s = \begin{cases} 1 & \text{if particle belongs to phase } s \\ 0 & \text{otherwise} \end{cases} \quad (17)$$

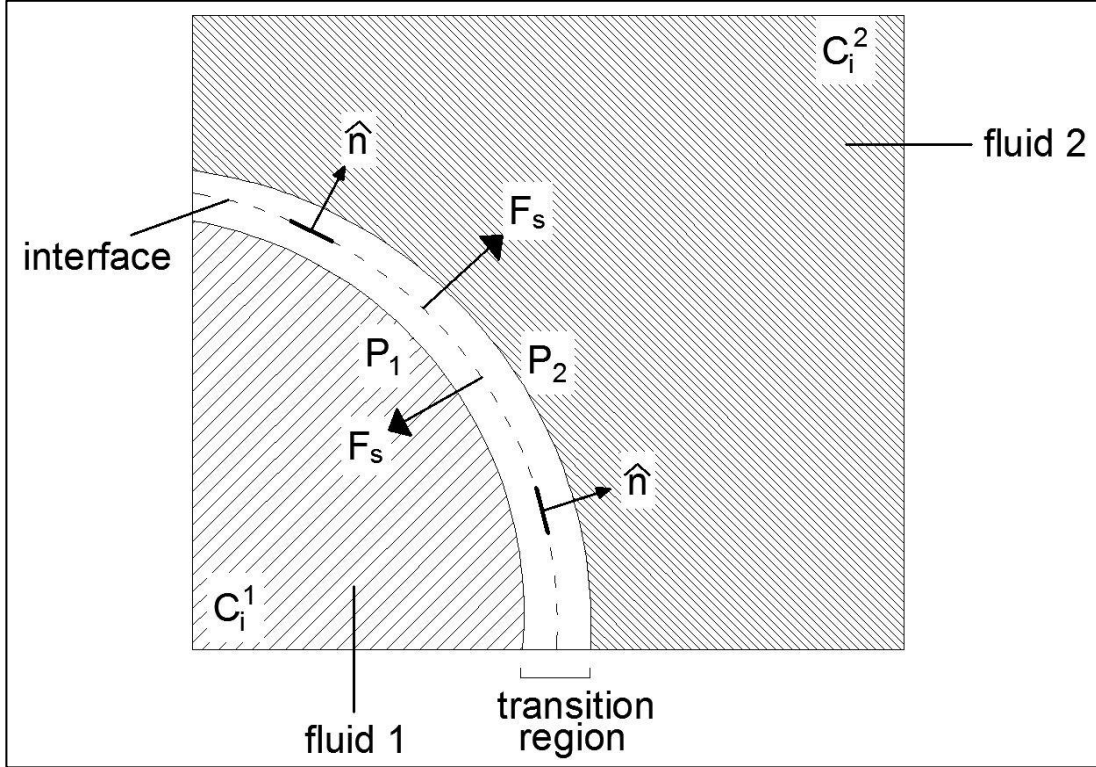


Figure 4: Sketch of continuum surface force (CSF) for phases 1 and 2

Hu and Adams [28] developed an approach to avoid the problem of particles far from the interface influencing the surface tension calculation by adopting the suggestion of Wu et al. [43], who expressed the shear stress contributions directly in terms of the color function gradients to calculate the surface tension.

The full momentum equation presented in Equation (10) can be rewritten as:

$$\begin{aligned} \frac{D\mathbf{v}_i}{Dt} = & - \sum_{j=1}^N m_j \left(\frac{P_i + P_j}{\rho_i \rho_j} + \Pi_{ij} \right) \nabla_i W_{ij} \\ & + \sum_{j=1}^N m_j \left(\frac{\Phi_i + \Phi_j}{\rho_i \rho_j} \right) \nabla_i W_{ij} + \mathbf{g} \end{aligned} \quad (18)$$

where the CSF term Φ is given in a tensor form [28].

3.3 Detection of Free-Surface Particles and Particle Shifting

In SPH simulations, the particle spatial arrangement can sometimes create situations where the particles are too close or too far from each other, leading to numerical instability. A variation of the particle shifting algorithm originally proposed by Xu et al. [44] for ISPH will be used to solve the stability and accuracy problems such as clumping due to irregular particle distributions.

The initial shifting algorithm of Xu et al. [44] has some significant problems such as noise in the pressure field inside the air bubble and also at the interface of the multi-phase, leading to stability problems in the simulation. Therefore, a treatment is necessary, especially for the air-water interface. A modified algorithm was proposed by Lind et al. [45] to change the shifting magnitude and direction according to Fick's law in order to obtain stable and accurate solutions for both internal and free-

surface flows. This will help the particles to be shifted by preventing highly anisotropic distributions. This behavior is expected for the air particles. Hence, shifting distance can be calculated as:

$$\delta \mathbf{r}_s = -D \nabla C_i \quad (19)$$

where $\delta \mathbf{r}_s$ denotes the shifting distance, D is a diffusion coefficient which controls the shifting magnitude and C_i is the particle concentration of particle i . The approach proposed by Skillen et al. [46] to calculate the diffusion coefficient has been used as:

$$D = -A_s h \|\mathbf{u}\|_i \Delta t \quad (20)$$

where A_s is a parameter taking a value from 1 to 6 and $\|\mathbf{u}\|_i$ is the velocity magnitude of the particle i . The value of A_s is the minimum possible value to present effective shifting. The recommended value of 2 has been used.

The particle concentration value can be calculated from the sum of the smoothing kernel function as:

$$C_i = \sum_{j=1}^N \frac{m_j}{\rho_j} W_{ij} \quad (21)$$

The concentration gradient can be found as in [47]:

$$\nabla C_i = \sum_{j=1}^N (C_j - C_i) \frac{m_j}{\rho_j} \nabla W_{ij} \quad (22)$$

As shown by Lind et al. [45] and Mokos et al. [48], a more uniform particle distribution has been obtained when this shifting method is introduced.

Modifications of the free-surface correction

Besides the treatments based on the concentration to determine the shifting distance and its direction explained above, Lind et al. [45] presented a correction method for the free-surface flows. Equation (19) shifts all the particles with a constant movement. Thus, the fluid particles at the interface are moved towards the interface to the air particles. This will result in mixing fluid and air particles together and creating instabilities. This has been seen in air bubble growth test cases with Xu et al. [44]'s shifting algorithm. In order to prevent unphysical mixing or movement at the interface, the concentration gradient near the surface should not be controlled by using global coordinates. Following from that, the binormal, tangent and normal vectors are considered for the 3-D model, allowing the shifting only in the tangent and binormal directions. Therefore, Equation (19) becomes [49]:

$$\delta \mathbf{r}_s = -D \left(\frac{\partial C_i}{\partial s} \hat{\mathbf{s}} + \frac{\partial C_i}{\partial b} \hat{\mathbf{b}} + \alpha_n \left(\frac{\partial C_i}{\partial n} - \beta_n \right) \hat{\mathbf{n}} \right) \quad (23)$$

where $\hat{\mathbf{s}}$, $\hat{\mathbf{n}}$ and $\hat{\mathbf{b}}$ are the tangent, normal and binormal vector respectively to the surface. β_n is a reference concentration gradient for the water phase in the free surface. The parameter α_n limits the diffusion in the normal direction, so the water particles are prevented from moving through the air particles. It is set to 0.1 in this study as air bubble modelling can be assumed as slow flows [45].

To identify free-surface particles, the divergence of particle position is used [50].

$$\nabla \cdot \mathbf{r} = \sum_{j=1}^N \frac{m_j}{\rho_j} \mathbf{r}_{ij} \cdot \nabla_i W_{ij} \quad (24)$$

This divergence of the particle position equals 2 for 2-D and 3 for 3-D simulations. Hence, for the 3-D simulations a threshold value of 2.5 is used to determine the particles belonging to the surface and

particle shifting is applied to the phases due to this value, i.e. if $\nabla \cdot \mathbf{r} < 2.5$, the particles are considered to belong to the surface.

In order to be effective and to obtain accurate results, Equation (19) has been performed for air particles so as to allow them to expand without mixing with the fluid phase. The same equation is also applied to the fluid particles, except it is applied at the interface. The treatment or surface correction term shown in Equation (23) has only been applied to the interface particles. This method was also conducted by Mokos et al. [49] to prevent the air phase dispersing in the water phase and creating voids.

3.4 Model Description

A single bubble expansion case has been simulated with the properties presented in Table 1. Fluid 1 and Fluid 2 represent the CO₂ gas inside the bubble and polymer melt surrounding the bubble respectively.

Table 1: The properties of the 3-D bubble growth model

Properties of the model	
Box dimension – L (m)	0.05
Radius of Fluid 1 – R (m)	0.01
Density of Fluid 1 (kg/m³)	1.9
Density of Fluid 2 (kg/m³)	1000
Speed of Sound of Fluid 1 (m/s)	30
Speed of Sound of Fluid 2 (m/s)	5
Surface tension coefficient - σ_s (N/m)	0.5
Gravity – g (m/s²)	0
Laminar viscosity	0.01 (water) 0.01 (air)

The surface tension effects are critical for bubble modelling and growth in microscale engineering problems especially for multi-phase problems with low flow. Running the SPH model at microscale (1 μm) proved to be unstable numerically. This is due to several factors, most notably that the denominator of α_d in Equation (5) is proportional to h^3 in 3-D. As h decreases to the microscale, this dependence on $1/h^3$ proves to be prohibitively unstable. Hence, simulations were performed at the millimeter scale to investigate the feasibility of modelling bubble growth. Surface tension effects should be scaled according to the relevant dimensionless numbers: namely Reynolds number, Bond number, Weber number, Capillary number and Marangoni number given by Bush [51]. Multi-phase bubble growth for herein this study in isothermal conditions is dominated by viscosity and surface tension effects so that capillary number scaling is the preferable option since it is based on the viscous and curvature forces given in Equation (25).

$$Ca = \frac{\rho v U}{\sigma_s} \quad (25)$$

where v is the viscosity of polymer, U is a characteristic speed as:

$$U = \sqrt{gR} \quad (26)$$

The Capillary number represents the ratio of viscous effects to surface tension (curvature) effects.

The surface tension coefficient ($\sigma_s = 0.028 \text{ N/m}^2$) given in the model parameters of Elshereef et al. [52] is for the bubble growth model of which the initial bubble radius is $1 \mu\text{m}$. At the micrometer scale, the Capillary number is $Ca = 447$. Therefore, the surface tension coefficient has been scaled by keeping the Capillary number constant, that is $(Ca)_{\mu\text{m}} = (Ca)_{\text{mm}}$, to simulate the bubble growth process at millimeter size.

The mass conversion from polymer melt to gas (mass loss) due to heat such as fire drives the expansion process by increasing the pressure inside the bubble. If the pressure inside the bubble is maintained, the volume of the bubble would have to increase as the mass of the gas phase increases. This mass transfer has been represented in SPH by increasing the number of gas particles inside the bubble during the simulation. The mass and the number of new gas particles have been estimated. The simulation of the single bubble growth model has been run up to 0.05 seconds. For an isothermal simulation duration of 0.05 s, the predicted expansion of a single bubble of initial radius 10 mm is 11 mm according to the model properties of Elshereef et al. [52] based on the analytical solution of Patel [25]. This expansion is driven by a mass transfer across the interface of $m_{transfer} = 2.74 \times 10^{-6} \text{ kg}$ of gas from the polymer melt into the bubble over a period of 0.05 seconds. In this simulation, it is assumed that the mass transfer occurs continuously throughout the simulation duration such that a certain number of new gas particles have been inserted into the bubble at regular intervals. For example, for a resolution of $\Delta x/R = 0.2$, the mass of a SPH gas particle, j , is $m_j = 1.52 \times 10^{-8} \text{ kg}$. Hence 180 ($= m_{transfer}/m_j$) new SPH gas particles need to be added to the bubble throughout the simulation. The rate of insertion of these particles is presented in the next section.

4 Results

The bubble growth model has been run with two different resolutions with $(\Delta x/R) = 0.2$ where the distance between the particles is 2 mm and $(\Delta x/R) = 0.1$ where the distance between the particles is 1 mm. Figure 5 shows the particle distribution of the bubble growth model, with the finer resolution $\Delta x/R = 0.1$, before and after conduction of the particle insertion method. In this simulation, 45 new gas particles have been inserted into the area close to the centre of the bubble every 0.01 seconds. Even though mass transfer takes place at the interface, adding particles at the centre of the bubble is satisfactory since the hydrodynamic conditions within the bubble for the timescales of this problem are uniform and steady. Identifying the location for new particles is not straightforward.

Special care has been taken not to generate a new gas particle at a position another gas particle has already occupied so as to prevent particle clumping. This is achieved by giving a random position to new gas particles using the FORTRAN RAND function. This function and position of a new gas particle in x, y and z-directions have been given as:

$$\begin{aligned} xp_{new} &= x_c + 0.25dx_0 + rand(0) \times 0.2dx_0 \\ yp_{new} &= y_c + 0.25dy_0 + rand(0) \times 0.2dy_0 \\ zp_{new} &= z_c + 0.25dz_0 + rand(0) \times 0.2dz_0 \end{aligned} \quad (27)$$

where xp_{new} , yp_{new} and zp_{new} are the positions of the new particle in three coordinates and x_c , y_c and z_c are the positions of the bubble centre while dx_0 , dy_0 and dz_0 are the distances between the particles. $rand(0)$ represents the RAND function in FORTRAN which has a value between 0 and 1. As new gas particles are introduced into the bubble, a slight expansion has been obtained at $t=0.01 \text{ s}$ as shown in Figure 5 (b). Therefore, the pressure inside the bubble increases while the outer pressure remains almost zero at 0.01 s.

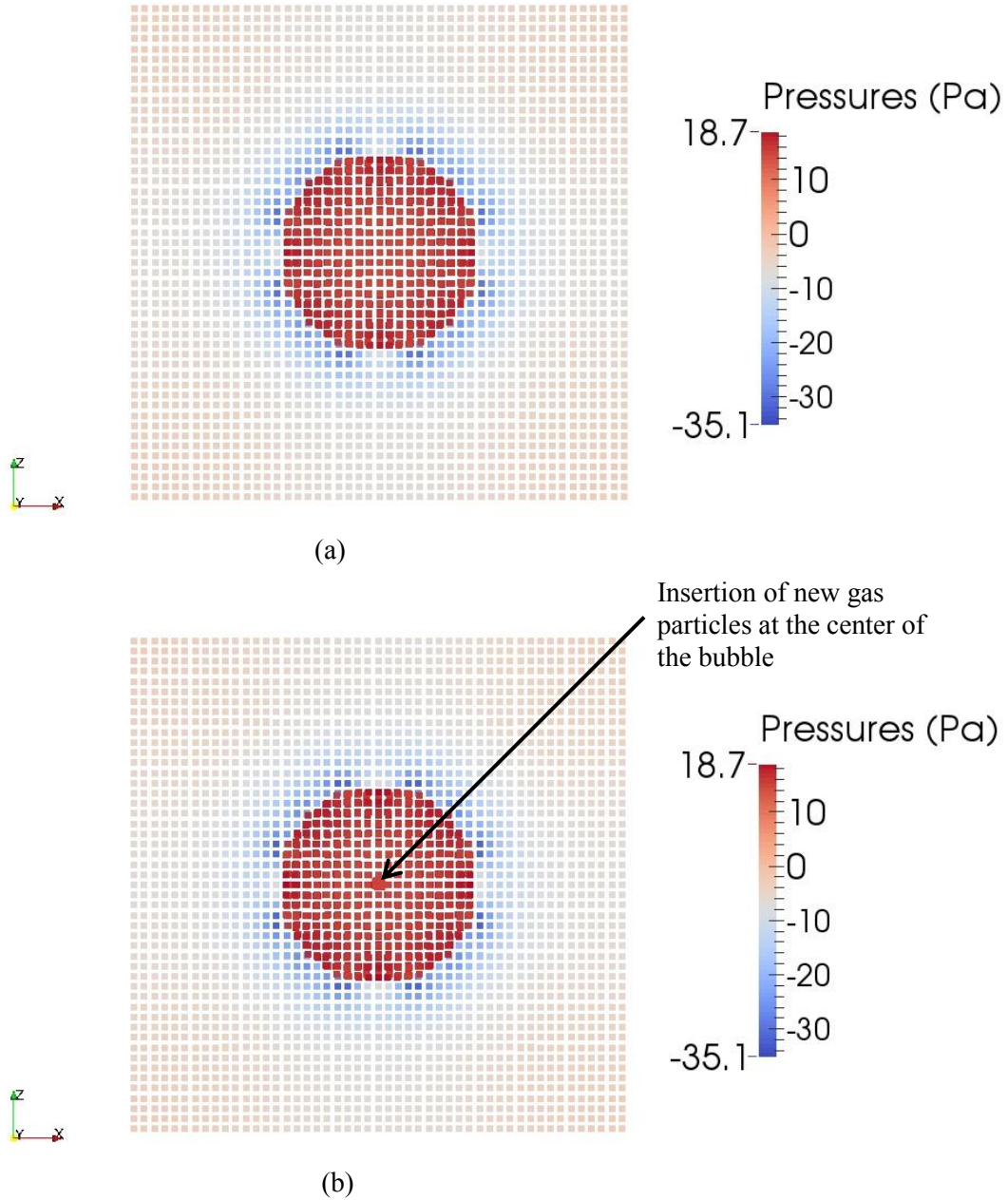


Figure 5: Particle distribution of the bubble growth model, (a) just before particle insertion at $t = 0.00996 \text{ s}$ (b) after particle insertion at $t = 0.01 \text{ s}$ (2-D slice at $y = 25 \text{ mm}$ from 3-D simulation)

Due to presence of the surface tension force, the shape of the bubble remains spherical as shown in Figure 6, which shows the final particle arrangements for the two resolutions. As the number of new gas particles increases further, the radius of the bubble increases as the air particles at the surface of the bubble push the water particles away at the surface. After the new particles' insertion, the particle distribution has been arranged according to the shifting algorithm explained in Section 3.3. However, the D (diffusion) parameter in Equation (19) has a significant effect on the shifting distance. Xenakis et al. [53] proposed a slightly modified shifting (diffusion) parameter to eliminate particle clumping in regions of low velocity, and this was implemented in the current code. However, it was found necessary to modify the proposal of Xenakis et al. [53] for the current application, to be given by:

$$\delta \mathbf{r}_s = \begin{cases} -A_s h \|\mathbf{u}\|_i \Delta t \nabla C_i & , D \geq D_0 \\ -D_0 \nabla C_i & , D < D_0 \\ -D_{min} \nabla C_i & , D < D_{min} \end{cases} \quad (28)$$

Therefore, the diffusion parameter D has been defined as a low threshold diffusion coefficient which takes a value of $D_0 = 0.01h^2$ and a minimum value of $D_{min} = 0.001h^2$ for this bubble expansion problem. In general for this model, particle shifting works satisfactorily herein and is also necessary for these kinds of multi-phase simulation where non-uniform deformations appear.

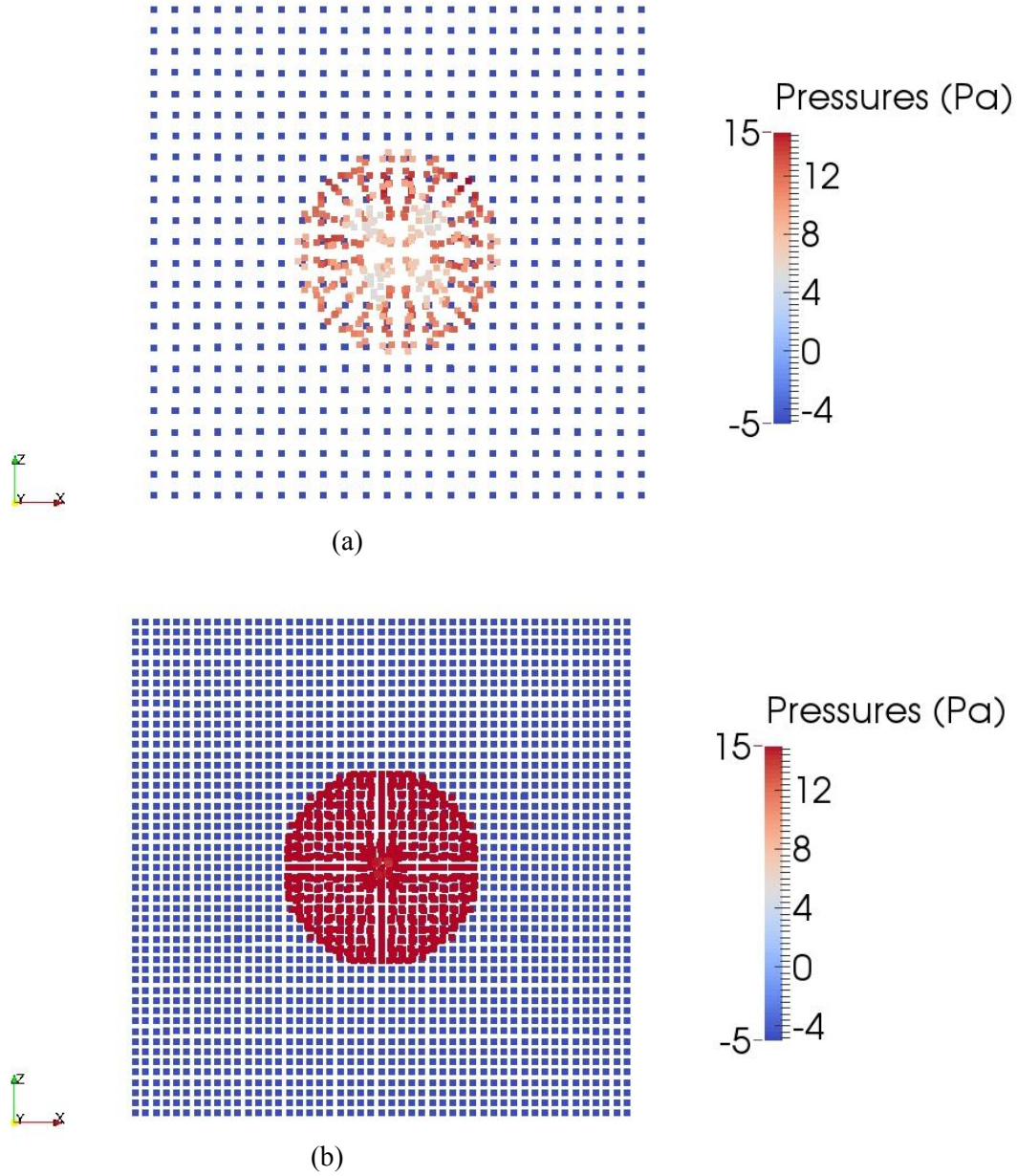


Figure 6: Expansion of the single bubbles at the end of the simulation (a) - Low resolution ($\Delta x/R = 0.2$) (b) - High resolution ($\Delta x/R = 0.1$)

As mentioned earlier, the simulation of the bubble modelling and expansion has been performed by insertion of new gas particles into the bubble at certain times. This particle insertion has been performed at regular intervals up to 0.05 seconds. Three simulations have been performed to identify the effect of the time period of particle insertion by inserting particles every 0.0025, 0.005 or 0.01 seconds. The radius of the bubble has been predicted using an algorithm tracking the surface particles

by considering a threshold value of 2.5 for the divergence of particle positions (Equation (24)). The radius is given by the average distance of the gas particles at the liquid-gas interface.

$$R(t) = \frac{1}{N} \sum_{i=1}^N r_i \quad (29)$$

where r_i is defined as all N gas particles where $r = \sqrt{(x_i - x_c)^2 + (y_i - y_c)^2 + (z_i - z_c)^2}$ for which $\nabla \cdot r_i < 2.5$.

However, as the bubble was not entirely spherical due to the resolution, the initial radius of the bubble was not exactly 10 mm. The initial value is approximately 8.9 mm for low resolution ($\Delta x/R = 0.2$) and 9.5 mm for high resolution ($\Delta x/R = 0.1$) simulations.

The comparison of the SPH bubble expansion with the analytical solution is shown in Figure 7. The predicted radius of the bubble has been shifted in time to have a comparison with the analytical solution of Patel [25] given in Section 2.1. There is no bubble growth observed until the new particle insertion algorithm performed at either 0.0025 s, 0.005 s or 0.01 s. Although there is a difference between the predicted bubble growth and analytical solution, this quite complex multi-phase algorithm presented the feasibility of bubble modelling and expansion using the SPH method.

Figure 7 shows a qualitatively appropriate expansion of the bubble with a difference due to the initial stages and particle insertion of the SPH simulation.

Figure 8 shows a comparison of the rate of the bubble expansion dR/dt predicted by SPH compared with theory. The theoretical bubble expansion rate is initially non-zero. The SPH results initially require a short to show an expansion rate but reach close agreement with theory by the end of the simulation. This agreement of the numerical results with the bubble expansion rate clearly demonstrates the potential of using SPH for polymer materials' expansion with chemical blowing agents. Figure 8 also shows that the rate of particle insertion has a limited effect, particularly for simulations longer than 0.05 seconds that are simulated here.

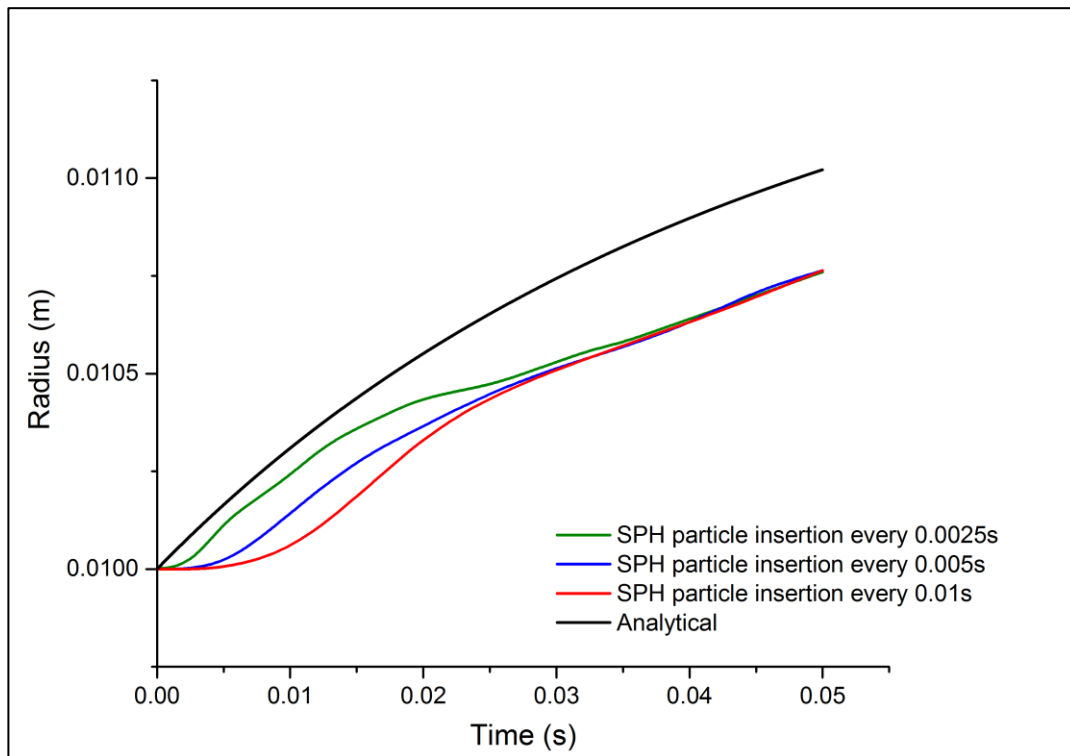


Figure 7: Comparison of the bubble growth between SPH modelling and analytical solution

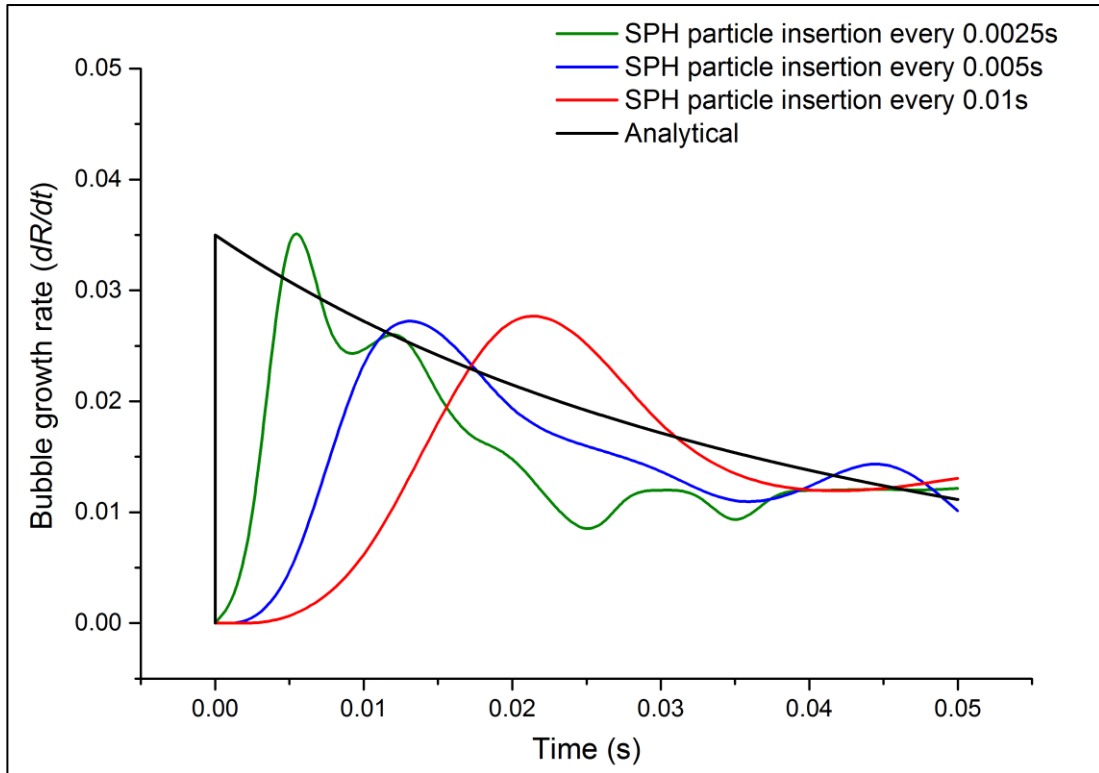


Figure 8: Comparison of bubble growth rates

In order to show numerical stability for the single bubble growth simulation, a time step analysis has been performed with a change of time. Figure 9 shows the change of time step (dt) with respect to time (t) when gas particles are inserted every 0.01 s. This demonstrates that the time step remains unchanged, being controlled by surface tension [42] until the new particles' introduction. With the new gas particles, the interaction and the forces between the particles increases as the distance between the particles would be less than the particle distance before insertion of new gas particles so that the time step is now controlled by viscous forces where interparticle distance is in the denominator, reducing Δt . Therefore, the time step reduces at 0.01, 0.02, 0.03 and 0.04 seconds based on the forces according to the variable time step.

Following the introduction of new particles, for example at $t = 0.01$ s, the shifting algorithm of Section 3.3 gradually rearranges the particles to have a more uniform distribution, which is demonstrated in the recovery of the time step by $t = 0.015$ s.

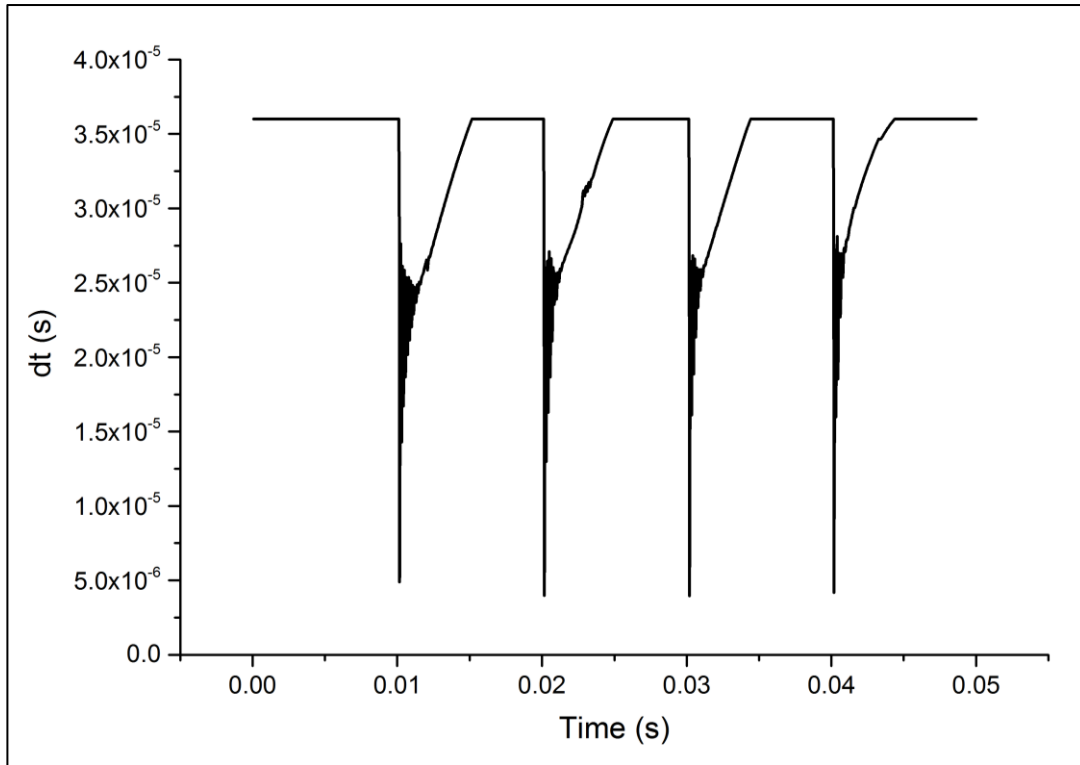


Figure 9: Change of time step (dt) with time (t)

To demonstrate the need for the new particle shifting routine, Figure 10 represents a particle distribution after performing the mass transfer without using the particle shifting. Even though the mass inside the bubble has been increased by particle insertion, shrinkage of the bubble can be observed. The newly inserted gas particles remain almost at the same positions where they are generated while the other gas particles move according to the momentum equation (compare to Figure 6a). Therefore, the shifting methodology is necessary for simulating bubble growth in multi-phase problems.

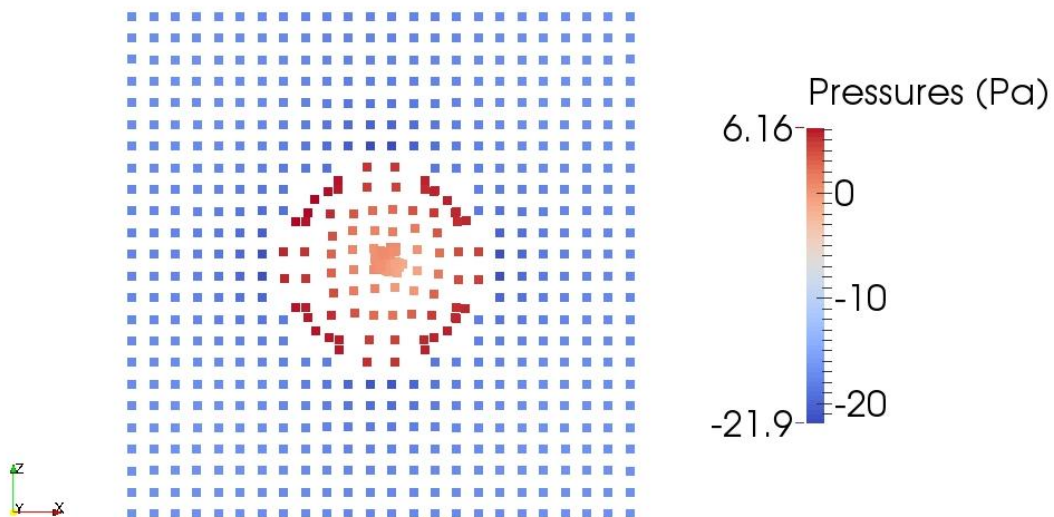


Figure 10: Particle distribution at $t = 0.05$ s without particle shifting ($\Delta x/R = 0.02$)

The main challenges of bubble growth modelling will be explained in the following section.

5 Conclusions

This paper has presented the feasibility of using the smoothed particle hydrodynamics (SPH) method to model the bubble growth process in a polymer material's expansion. A single gas bubble's growth in surrounding liquid has been developed and the main challenges in terms of the SPH approach have been identified and discussed. A new SPH algorithm for representing the mass conversion has been performed to predict and simulate the single bubble expansion with and without shifting algorithm. It can be concluded that the shifting algorithm has a great influence on the bubble growth as shrinkage occurs without shifting.

The SPH multi-phase model has been validated against an analytical solution. The major advantage of using SPH to simulate the multi-phase models compared to other mesh-based computational methods is that the highly non-linear and non-uniform behavior of the motion at the interface (e.g. interface between polymer melt and gas in this project) can easily be captured without any requirement to generate a mesh. For the new approach, particle insertion to represent the mass conversion showed that this new SPH model can be applicable for the bubble expansion simulations with further improvements required for efficient, accurate and stable multi-phase simulations.

References

- [1] J.J. Feng and C.A. Bertelo. *Prediction of bubble growth and size distribution in polymer foaming based on a new heterogeneous nucleation model*. Journal of Rheology, 48(2): 439, 2004.
- [2] A. Naber, C. Liu, and J.J. Feng, *The Nucleation and Growth of Gas Bubbles in a Newtonian Fluid: An Energetic Variational Phase Field Approach*, in *Moving Interface Problems and Applications in Fluid Dynamics*, B.C. Khoo, Z. Li, and P. Lin, Editors. 2008, Contemporary Mathematics. p. 95-120.
- [3] T.R. Tuladhar and M.R. Mackley. *Experimental observations and modelling relating to foaming and bubble growth from pentane loaded polystyrene melts*. Chemical Engineering Science, 59(24): 5997-6014, 2004.
- [4] M. Amon and C.D. Denson. *A study of the dynamics of foam growth: Analysis of the growth of closely spaced spherical bubbles*. Polymer Engineering & Science, 24(13): 1026-1034, 1984.
- [5] M.R. Pivello, M.M. Villar, R. Serfaty, A.M. Roma, and A. Silveira-Neto. *A fully adaptive front tracking method for the simulation of two phase flows*. International Journal of Multiphase Flow, 58: 72-82, 2014.
- [6] N. Balcázar, O. Lehmkuhl, J. Rigola, and A. Oliva. *A multiple marker level-set method for simulation of deformable fluid particles*. International Journal of Multiphase Flow, 74(0): 125-142, 2015.
- [7] S.J. Lind and T.N. Phillips. *Bubble collapse in compressible fluids using a spectral element marker particle method. Part 2. Viscoelastic fluids*. International Journal for Numerical Methods in Fluids, 71(9): 1103-1130, 2013.
- [8] Q. Zeng, J. Cai, H. Yin, X. Yang, and T. Watanabe. *Numerical simulation of single bubble condensation in subcooled flow using OpenFOAM*. Progress in Nuclear Energy, 83(0): 336-346, 2015.
- [9] M. Cheng, J. Hua, and J. Lou. *Simulation of bubble–bubble interaction using a lattice Boltzmann method*. Computers & Fluids, 39(2): 260-270, 2010.
- [10] M. van Sint Annaland, N.G. Deen, and J.A.M. Kuipers. *Numerical simulation of gas bubbles behaviour using a three-dimensional volume of fluid method*. Chemical Engineering Science, 60(11): 2999-3011, 2005.
- [11] G.R. Liu and M.B. Liu, *Smoothed Particle Hydrodynamics A Meshfree Particle Method*. 2003, Sinagapore: World Scientific Publishing. 449.
- [12] R.A. Gingold and J.J. Monaghan. *Smoothed particle hydrodynamics: theory and application to non-spherical stars*. Monthly Notices of the Royal Astronomical Society, 181: 375-398, 1977.
- [13] L.B. Lucy. *A numerical approach to the testing of the fission hypothesis*. The Astronomical Journal, 82(12): 1013-1024, 1977.
- [14] N. Katz. *Dissipational galaxy formation. II - Effects of star formation*. Astrophysical Journal, 391(2): 502-517, 1992.
- [15] V. Springel. *Smoothed Particle Hydrodynamics in Astrophysics*. Annual Review of Astronomy and Astrophysics, 48(1): 391-430, 2010.
- [16] J.J. Monaghan and A. Kos. *Solitary waves on a Creatan beach*. Journal of Waterway, Port, Coastal, and Ocean Engineering, 125: 145-154, 1999.
- [17] J.J. Monaghan. *Simulating Free Surface Flows with SPH*. Journal of Computational Physics, 110(2): 399-406, 1994.
- [18] D. Violeau and B.D. Rogers. *Smoothed particle hydrodynamics (SPH) for free-surface flows: past, present and future*. Journal of Hydraulic Research, 54(1): 1-26, 2016.
- [19] W. Benz and E. Asphaug. *Impact Simulations with Fracture. I. Method and Tests*. Icarus, 107(1): 98-116, 1994.
- [20] W. Benz and E. Asphaug. *Simulations of brittle solids using smooth particle hydrodynamics*. Computer Physics Communications, 87(1–2): 253-265, 1995.
- [21] J.H. Jeong, M.S. Jhon, J.S. Halow, and J. van Osdol. *Smoothed particle hydrodynamics: Applications to heat conduction*. Computer Physics Communications, 153(1): 71-84, 2003.

- [22] C. Antoci, M. Gallati, and S. Sibilla. *Numerical simulation of fluid–structure interaction by SPH*. *Computers & Structures*, 85(11–14): 879-890, 2007.
- [23] R.A. Dalrymple and B.D. Rogers. *Numerical modeling of water waves with the SPH method*. *Coastal Engineering*, 53(2–3): 141-147, 2006.
- [24] A. Colagrossi and M. Landrini. *Numerical simulation of interfacial flows by smoothed particle hydrodynamics*. *Journal of Computational Physics*, 191(2): 448-475, 2003.
- [25] R.D. Patel. *Bubble growth in a viscous Newtonian liquid*. *Chemical Engineering Science*, 35: 2352-2356, 1980.
- [26] M. Sussman, P. Smereka, and S. Osher. *A Level Set Approach for Computing Solutions to Incompressible Two-Phase Flow*. *Journal of Computational Physics*, 114(1): 146-159, 1994.
- [27] J.J. Monaghan, *Smoothed particle hydrodynamics*, in *Reports on Progress in Physics*. 2005, Institute of Physics Publishing, p. 1703-1759.
- [28] X.Y. Hu and N.A. Adams. *A multi-phase SPH method for macroscopic and mesoscopic flows*. *Journal of Computational Physics*, 213(2): 844-861, 2006.
- [29] X.Y. Hu and N.A. Adams. *An incompressible multi-phase SPH method*. *Journal of Computational Physics*, 227(1): 264-278, 2007.
- [30] J.J. Monaghan and A. Kocharyan. *SPH simulation of multi-phase flow*. *Computer Physics Communications*, 87(1–2): 225-235, 1995.
- [31] X.Y. Hu and N.A. Adams. *A constant-density approach for incompressible multi-phase SPH*. *Journal of Computational Physics*, 228(6): 2082-2091, 2009.
- [32] N. Grenier, M. Antuono, A. Colagrossi, D. Le Touzé, and B. Alessandrini. *An Hamiltonian interface SPH formulation for multi-fluid and free surface flows*. *Journal of Computational Physics*, 228(22): 8380-8393, 2009.
- [33] J.J. Monaghan. *A simple and efficient algorithm for multi-fluids*. in *6th International SPHERIC Workshop*. 2011. Hamburg, Germany.
- [34] J.J. Monaghan and A. Rafiee. *A simple SPH algorithm for multi-fluid flow with high density ratios*. *International Journal for Numerical Methods in Fluids*, 71(5): 537-561, 2013.
- [35] P. Sun, A. Zhang, and F. Ming. *3D SPH simulation of bubble rising and coalescing in viscous fluids*. in *10th International SPHERIC Workshop*. 2015. Parma, Italy.
- [36] K. Szewc, J. Pozorski, and J.P. Minier. *Simulations of single bubbles rising through viscous liquids using Smoothed Particle Hydrodynamics*. *International Journal of Multiphase Flow*, 50: 98-105, 2013.
- [37] M. Gomez-Gesteira, B.D. Rogers, R.A. Dalrymple, A.J.C. Crespo, and M. Narayanaswamy. *User Guide for the SPHysics code*. 2010; 2.2:[Available from: <http://wiki.manchester.ac.uk/sphysics>].
- [38] M. Gomez-Gesteira, B.D. Rogers, A.J.C. Crespo, R.A. Dalrymple, M. Narayanaswamy, and J.M. Dominguez. *SPHysics – development of a free-surface fluid solver – Part 1: Theory and formulations*. *Computers & Geosciences*, 48(0): 289-299, 2012.
- [39] J.P. Morris, P.J. Fox, and Y. Zhu. *Modeling Low Reynolds Number Incompressible Flows Using SPH*. *Journal of Computational Physics*, 136(1): 214-226, 1997.
- [40] J.J. Monaghan. *Smoothed Particle Hydrodynamics*. *Astronomy and Astrophysics*, 30: 543-574, 1992.
- [41] M. Gomez-Gesteira, A.J.C. Crespo, B.D. Rogers, R.A. Dalrymple, J.M. Dominguez, and A. Barreiro. *SPHysics – development of a free-surface fluid solver – Part 2: Efficiency and test cases*. *Computers & Geosciences*, 48(0): 300-307, 2012.
- [42] J.U. Brackbill, D.B. Kothe, and C. Zemach. *A Continuum Method for Modelling Surface Tension*. *Journal of Computational Physics*, 100: 335-354, 1992.
- [43] J. Wu, S.-T. Yu, and B.-N. Jiang. *Simulation of two-fluid flows by the least-squares finite element method using a continuum surface tension model*. *International Journal for Numerical Methods in Engineering*, 42(4): 583-600, 1998.
- [44] R. Xu, P. Stansby, and D. Laurence. *Accuracy and stability in incompressible SPH (ISPH) based on the projection method and a new approach*. *Journal of Computational Physics*, 228(18): 6703-6725, 2009.
- [45] S.J. Lind, R. Xu, P.K. Stansby, and B.D. Rogers. *Incompressible smoothed particle hydrodynamics for free-surface flows: A generalised diffusion-based algorithm for stability and*

- validations for impulsive flows and propagating waves.* Journal of Computational Physics, 231(4): 1499-1523, 2012.
- [46] A. Skillen, S. Lind, P.K. Stansby, and B.D. Rogers. *Incompressible smoothed particle hydrodynamics (SPH) with reduced temporal noise and generalised Fickian smoothing applied to body–water slam and efficient wave–body interaction.* Computer Methods in Applied Mechanics and Engineering, 265(0): 163-173, 2013.
- [47] A. Mokos, *Multi-phase Modelling of Violent Hydrodynamics Using Smoothed Particle Hydrodynamics (SPH) on Graphics Processing Units (GPUs)*, in *Faculty of Engineering and Physical Sciences*. 2013, University of Manchester: Manchester. p. 250.
- [48] A. Mokos, B.D. Rogers, P.K. Stansby, and J.M. Domínguez. *Multi-phase SPH modelling of violent hydrodynamics on GPUs.* Computer Physics Communications, 196: 304-316, 2015.
- [49] A. Mokos, B. Rogers, and P.K. Stansby. *A Multi-Phase Particle Shifting Algorithm for SPH Simulations of Violent Hydrodynamics for Large Numbers of Particles.* Journal of Hydraulic Research, 2016.
- [50] E.S. Lee, C. Moulinec, R. Xu, D. Violeau, D. Laurence, and P. Stansby. *Comparisons of weakly compressible and truly incompressible algorithms for the SPH mesh free particle method.* Journal of Computational Physics, 227(18): 8417-8436, 2008.
- [51] J.W.M. Bush, *Interfacial Phenomena*. 2013, Massachusetts Institute of Technology MIT. p. 1-81.
- [52] R. Elshereef, J. Vlachopoulos, and A. Elkamel. *Comparison and analysis of bubble growth and foam formation models.* Engineering Computations, 27(3): 387-408, 2010.
- [53] A.M. Xenakis, S.J. Lind, P.K. Stansby, and B.D. Rogers. *An ISPH scheme with shifting for Newtonian and non-Newtonian multi-phase flows.* in *10th International SPHERIC Workshop*. 2015. Parma, Italy.